3DMKDSRC: A NOVEL APPROACH FOR 3D FACE RECOGNITION

*Lin Zhang, Zhixuan Ding, Hongyu Li**

School of Software Engineering
Tongji University
Shanghai 201804, China

Jianwei Lu

Institute of Advanced Translational Medicine
& School of Software Engineering
Tongji University, Shanghai 201804, China

ABSTRACT

Recent years have witnessed a growing interest in developing methods for 3D face recognition. However, 3D scans often suffer from the problems of missing parts, large facial expressions, and occlusions. In this paper, we propose a novel general approach to deal with the 3D face recognition problem by making use of multiple keypoint descriptors (MKD) and the sparse representation-based classifier (SRC). We call the proposed method 3DMKDSRC for short. Specifically, with 3DMKDSRC, each 3D face scan is represented as a set of descriptor vectors extracted from keypoints by meshSIFT. Descriptor vectors of gallery samples form the gallery dictionary. Given a probe 3D face scan, its descriptors are extracted at first and then its identity can be determined by using a multitask SRC. The effectiveness of 3DMKDSRC has been corroborated by extensive experiments.

Index Terms— 3D face recognition, meshSIFT, sparse representation, biometrics, keypoint descriptor

1. INTRODUCTION

The face has many benefits when compared to other biometrics. Face recognition using 2D images is still a great challenge due to kinds of adverse factors, such as illumination variation, pose changes, and facial expressions. By contrast, 3D scanning has a major advantage over 2D imaging in that those nuisance factors have a relatively smaller influence.

To enable efficient matching of 3D faces, facial data should be represented in an appropriate manner. To this end, researchers have proposed kinds of schemes. Several holistic representation methods are at first proposed. In [1], Dorai *et al*. proposed an algorithm called Curvedness-Orientation-Shape Map On Shape (COSMOS). In [1], shape information such as surface area, curvedness, and connectivity are integrated in terms of maximal surface patches of constant shape index. In [2], Mian *et al*. proposed a spherical face representation approach, in which point cloud of 3D facial data is quantized into spherical bins rather than 3D grids. Smeets *et al*. in [3] proposed a geodesic distance matrix (GDM)-based representation scheme, in which the vector of eigenvalues of GDM is used as an isometry-invariant shape representation.

The non-rigid deformations due to facial expressions, missing data, and self-occlusion problems caused in data acquisition severely affect the accuracy of 3D face recognition. To cope with these issues, many researchers turned to matching methods based on local representations. In [4], Chua *et al*. proposed a point signature method and used it for representing 3D faces with non-neutral expressions. In [5], Husken *et al*. proposed a multimodal method using 2D and 3D hierarchical graph matching (HGM). The HGM worked as an elastic graph storing local features in its nodes, and structural information in its edges. In [6], Wang *et al*. used a signed shape-difference map between two aligned 3D faces as an intermediate representation for shape comparison. Inspired by SIFT [7], Smeets *et al*. [8] developed a meshSIFT algorithm which could detect keypoints and build local descriptors for 3D meshes. Such an algorithm has been applied to 3D face recognition and promising results were reported on Bosphorus database [9].

Sparse representation as an effective classification tool [10] has also been introduced to the biometrics field. The seminal work of Wright *et al*. [10] has demonstrated that the sparse representation-based classifier (SRC) is an effective framework for 2D face recognition. Quite recently, Liao *et al.* proposed an alignment-free 2D partial face matching approach MKDSRC, in which each face is represented by a set of descriptor vectors extracted from keypoints and a multitask SRC is used for classification [11]. Such a method can address the problem of 2D partial face matching pretty well.

When missing data, large facial expressions, or occlusions exist in 3D face scans, it would be difficult for an approach based on holistic representations to succeed. Instead, methods resorting to local representations seem more appealing. Inspired by the great success of MKDSRC [11] designed for 2D face matching, in this paper, we propose a novel general 3D face recognition scheme based on local representations. Specifically, for each 3D face scan $\mathcal{F}$, we at first use meshSIFT [8] to extract from it multiple keypoints and then build the associated local descriptors. Such a set of local descriptors can be used as a representation of $\mathcal{F}$. To build the

*Corresponding author. Email: hyli@tongji.edu.cn

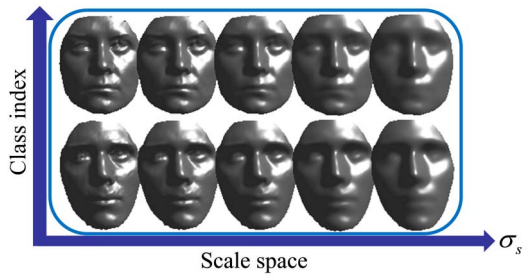

Fig. 1. Shapes of two face scans in the scale space.

gallery dictionary, all the local descriptors extracted from the gallery samples are concatenated together. Given a probe face scan, its local descriptors are extracted at first and then its identity can be determined by using a multi-task SRC. The proposed method is called 3DMKDSRC (3D Multiple Keypoint Descriptors and Sparse Representation-based Classifier). 3DMKDSRC uses a variable-size description and accordingly each face scan is represented by a set of descriptors. Since the MKD dictionary comprises a large number of gallery descriptors, it is highly possible to sparsely represent descriptors from a probe scan, irrespective of whether it is a holistic, partial, or occluded one. 3DMKDSRC is particulary appropriate for matching 3D scans with missing parts, facial expressions, or occlusions. Its efficacy has been validated on three widely used benchmark databases.

The rest of this paper is organized as follows. Section 2 briefly reviews meshSIFT. Section 3 presents our 3DMKDSRC in details. Section 4 reports the experimental results while Section 5 concludes the paper.

2. MESHSIFT

In our 3DMKDSRC approach, each 3D face scan is represented by a set of local descriptors extracted from keypoints. With respect to the scheme for keypoint detection and local descriptor construction for 3D scans, we resort to meshSIFT [8], which is an effective method designed for these particular tasks proposed quite recently. MeshSIFT was highly motivated by SIFT [7], which is now a widely used method to build scale invariant local descriptors for 2D gray-scale images. In this section, we briefly review the key steps of meshSIFT.

2.1. Keypoint detection

The keypoint detection step in meshSIFT is similar to SIFT. A scale space containing smoothed versions of the input mesh is constructed at first as:

$$M_s = \begin{cases} M, \text{ if } s = 0 \\ \widehat{G}_{\sigma_s} \otimes M, \ else \end{cases} \tag{1}$$

where M stands for the original mesh, $\otimes$ stands for the convolution operation, and $\hat{G}_{\sigma_s}$ stands for the approximated Gaussian filter with scale σ_s. These scales $\{\sigma_s\}$ vary exponentially

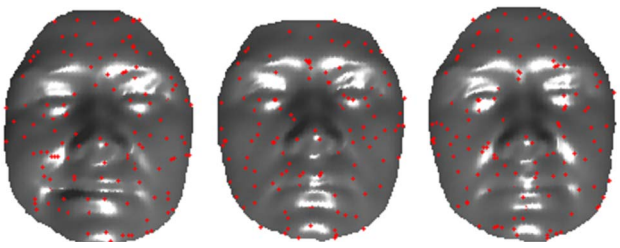

Fig. 2. Keypoint detection results on three face scans of the same face.

as $\sigma_s = 2^{\frac{s}{k}}\sigma_0$, where k stands for the number of total scales. Since the number of convolutions is discrete, σ_s is approximated as:

$$\widetilde{\sigma}_s = \overline{e}\sqrt{\frac{2\sigma_0}{3}}2^{\frac{s}{k}} \tag{2}$$

with $\overline{e}$ the average edge length. Fig. 1 shows the shapes of two face scans in the scale space.

To detect keypoints in the scale space, the mean curvature is computed for each vertex *i* at each scale *s* as:

$$H_i^s = \frac{k_{i,1}^s + k_{i,2}^s}{2} \tag{3}$$

where $k_{i,1}^s$ and $k_{i,2}^s$ respectively stand for the maximum and minimum curvature for each vertex *i* at scale *s*. The difference between subsequent scales could be computed as:

$$dH_i^s = H_i^{s+1} - H_i^s \tag{4}$$

A vertex is selected as a keypoint only when its value dH_i^s is larger or smaller than all its neighboring vertices in all upper, current, and lower scales. The scale σ_s at which the extremum is obtained is assigned to each keypoint. Fig. 2 shows an example of keypoint detection results of 3 face scans collected from the same person.

2.2. Local descriptor

Having detected keypoints, the next step is to describe them with local descriptors which actually summarise the local neighborhood information around them. In order to obtain an orientation-invariant descriptor, each keypoint is assigned a canonical orientation. With such a canonical orientation, it is possible to construct a local reference frame in which the vertices of the neighborhood can be expressed independent of the facial pose.

For a keypoint P, all vertices within a spherical region of radius $9\sigma_s$ around it are its neighboring points. The normal vectors of these points are projected onto the tangent plane of the mesh containing P. The projected normal vectors are gathered in a weighted histogram with 360 bins. Each histogram entry is Gaussian weighted with the geodesic distances to P. The highest peak in the histogram and the peaks above 80% of this highest peak value are selected as canonical

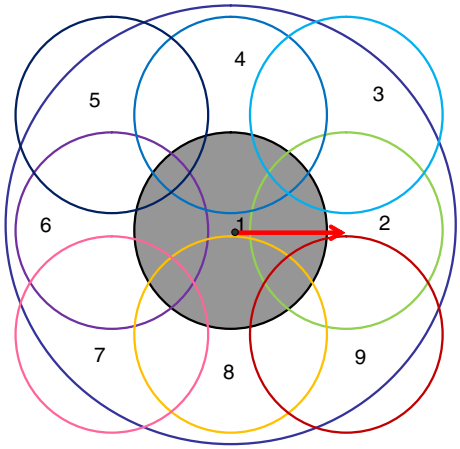

Fig. 3. 9 regions involved in the computation of the local descriptor. The red arrow indicates the canonical orientation.

orientations. For a keypoint which has more than one canonical orientations, it can be regarded as multiple keypoints, each assigned one of the canonical orientations.

The generation of a local descriptor for P is based on 9 sub-regions. As described in Fig. 3, the locations of these 9 regions are based on the canonical orientation of P. The geodesic distances from the centers of regions 2, 4, 6 and 8 to P are all $4.5\sigma_s$, while the geodesic distances from the centers of regions 3, 5, 7 and 9 to P are all $4.5\sqrt{2}\sigma_s$.

For each of the 9 regions, two histograms p_S and p_θ are used for generating the descriptor. The first histogram contains the shape index which is expressed as:

$$S_i = \frac{2}{\pi}\tan^{-1}\left(\frac{k_{i,1}+k_{i,2}}{k_{i,1}-k_{i,2}}\right) \tag{5}$$

where $k_{i,1}$ and $k_{i,2}$ are the maximum and the minimum curvatures, respectively. The second histogram contains the slant angles, which are defined as the angles between the projected normals and the canonical orientation. Both the shape index and the slant angle histograms are Gaussian weighted with the geodesic distances to P. Finally, the histograms are concatenated in a vector form as $\boldsymbol{f} = [p_{S,1}p_{\theta,1}...p_{S,9}p_{\theta,9}]^T$ and $\boldsymbol{f}$ is regarded as the descriptor of P. Consequently, each 3D face scan can be represented as a set of descriptor vectors $\mathbf{F} = [\boldsymbol{f}_1, \ldots, \boldsymbol{f}_n]$, where each $\boldsymbol{f}_i$ is a local descriptor vector.

3. 3DMKDSRC

In this section, the proposed 3D face recognition scheme 3DMKDSRC will be presented in details.

3.1. Construction of the gallery dictionary

For each sample scan in the gallery set, its local descriptors could be computed by meshSIFT. Then, the gallery dictionary is constructed by concatenating these descriptors together. Suppose that there are C subjects in gallery and for each subject i there are totally n_i derived descriptors. Usually, these n_i descriptors are obtained from multiple samples of the subject i. For the i^{th} subject, let

$$\mathbf{D}_i = [\boldsymbol{s}_{i,1}, \boldsymbol{s}_{i,2}, ..., \boldsymbol{s}_{i,n_i}] \in \mathcal{R}^{m\times n_i} \tag{6}$$

where m here stands for the descriptor dimension. The gallery dictionary $\mathbf{D}$ can be simply constructed by concatenating these $\mathbf{D}_i$s as:

$$\mathbf{D} = [\mathbf{D}_1, \mathbf{D}_2, ..., \mathbf{D}_C] \in \mathcal{R}^{m\times K} \tag{7}$$

where K here represents the total number of descriptors in the gallery set. Typically, K is very large, making $\mathbf{D}$ an overcomplete description space of the C classes.

3.2. Multitask sparse representation

Given a probe 3D face scan, we at first compute from it a set of local descriptors:

$$\mathbf{Y} = (\boldsymbol{y}_1, \boldsymbol{y}_2, ..., \boldsymbol{y}_n) \tag{8}$$

with n the number of keypoints detected from this scan. Then, the sparse representation problem is formulated as:

$$\widehat{\mathbf{X}} = \arg\min_{\mathbf{X}} \sum_{i=1}^{n} \|\boldsymbol{x}_i\|_0, \ s.t.\ \mathbf{Y} = \mathbf{DX} \tag{9}$$

where $\mathbf{X} = (\boldsymbol{x}_1, \boldsymbol{x}_2, ..., \boldsymbol{x}_n) \in \mathcal{R}^{K\times n}$ is the sparse coefficient matrix, and $\|\cdot\|_0$ denotes the l_0-norm of a vector. However, the solution to this problem is NP-hard. As suggested by the research results of compressed sensing [12], sparse signals can be well recovered with a high probability via the l_1-minimization. Therefore, Eq.(9) can be approximated by:

$$\widehat{\mathbf{X}} = \arg\min_{\mathbf{X}} \sum_{i=1}^{n} \|\boldsymbol{x}_i\|_1, \ s.t.\ \mathbf{Y} = \mathbf{DX} \tag{10}$$

where $\|\cdot\|_1$ represents the l_1-norm of the vector. This is a multitask problem as both $\mathbf{X}$ and $\mathbf{Y}$ have multiple columns. Equivalently, we can solve the following set of n l_1-minimization problems, one for each probe descriptor $\boldsymbol{y}_i$:

$$\widehat{\boldsymbol{x}}_i = \arg\min_{\boldsymbol{x}_i} \|\boldsymbol{x}_i\|_1, \ s.t.\ \boldsymbol{y}_i = \mathbf{D}\boldsymbol{x}_i, i = 1, 2, ..., n \tag{11}$$

To solve Eq.(11), we use the Homotopy algorithm proposed in [13]. Usually, if the identity of the probe face scan is covered by the gallery set, the coefficient vectors of its local descriptors would be very sparse as illustrated in Fig. 4.

Inspired by [10, 11], we adopt the following multitask SRC to determine the identity of the probe face scan:

$$identity(\mathbf{Y}) = \arg\min_{c} \sum_{i=1}^{n} \|\boldsymbol{y}_i - \mathbf{D}\delta_c(\widehat{\boldsymbol{x}}_i)\|_2 \tag{12}$$

where $\delta_c(\cdot)$ is a function which selects only the coefficients corresponding to class c. Eq.(12) makes use of the sum of reconstruction residuals of the n descriptors with respect to each class to determine the identity of the input face scan.

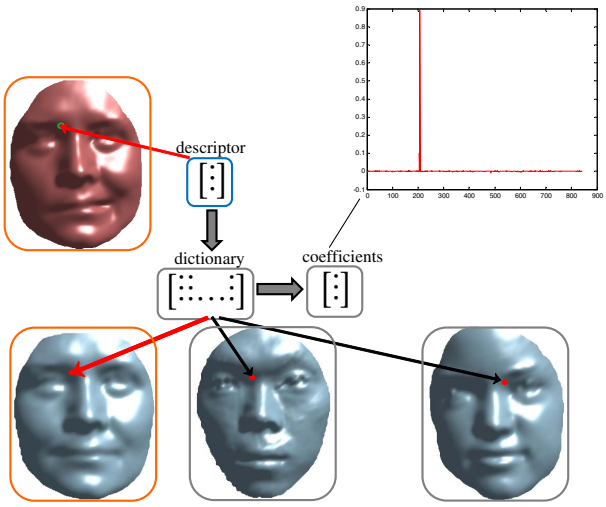

Fig. 4. If a query descriptor has a matched descriptor in gallery, the coefficient would be very sparse.

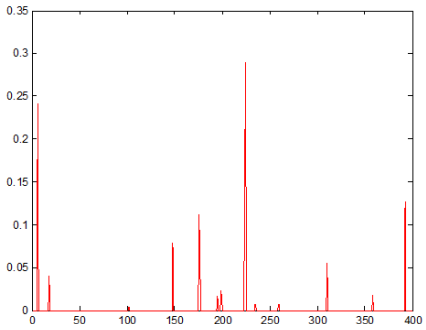

Fig. 5. An example of a coefficient vector which is not sparse.

3.3. Dictionary shrinking and sparsity criterion

In practice, the size (K) of the dictionary can be extremely large, making it difficult to solve Eq.(11). Hence, we adopt a similar idea as Liao *et al*. [11] to derive a fast approximate solution. For each probe descriptor $\boldsymbol{y}_i$, we first compute:

$$\boldsymbol{d}_i = \mathbf{D}^T \boldsymbol{y}_i \tag{13}$$

Then, for each $\boldsymbol{y}_i$, we only keep $L(L << K)$ descriptors in $\mathbf{D}$ according to the L largest values of $\boldsymbol{d}_i$, resulting in a small sub-dictionary $\mathbf{D}^{(i)}_{m\times L}$. Then, $\mathbf{D}$ is replaced by $\mathbf{D}^{(i)}$ in Eq.(11) and Eq.(12) is adjusted accordingly. In our implementation, L is set to 400.

In addition, we assume that if the identity of the probe face scan belongs to the j^{th} subject of the gallery, the entries of $\widehat{\boldsymbol{x}}_i$ should be small except those associated with the j^{th} subject. If the coefficients $\widehat{\boldsymbol{x}}_i$ are not concentrated on any subject and instead values of $\widehat{\boldsymbol{x}}_i$ spread evenly over all the gallery subjects, $\boldsymbol{y}_i$ is likely to be a noisy descriptor and it can provide little discriminative information. Thus, such $\widehat{\boldsymbol{x}}_i$s will not be considered when computing Eq.(12).

To evaluate the sparsity of $\widehat{\boldsymbol{x}}_i$, we use,

$$sparsity(\widehat{\boldsymbol{x}}_i) = \frac{k \times Main(\widehat{\boldsymbol{x}}_i)/\|\widehat{\boldsymbol{x}}_i\|_1 - 1}{k-1} \tag{14}$$

where k is the number of subjects in $\mathbf{D}^{(i)}$ and $Main(\widehat{\boldsymbol{x}}_i)$ stands for the summation of absolute values of coefficients in $\widehat{\boldsymbol{x}}_i$ corresponding to the first 5 percent of subjects with higher sums of absolute coefficients. If $sparsity(\widehat{\boldsymbol{x}}_i)$ is larger than a threshold (0.8 in our implementation), we consider that $\widehat{\boldsymbol{x}}_i$ is sparse enough and it will be involved in the further determination of identity (see Eq.(12)). Fig. 5 shows an example of the distribution of a coefficient vector which is not sparse.

The overall pipeline of our proposed 3DMKDSRC algorithm is illustrated in Fig. 6.

4. EXPERIMENTAL RESULTS AND DISCUSSIONS

4.1. Experiments on Bosphorus

The Bosphorus database [9] consists of 4666 facial range scans from 105 different subjects and is acquired by an Inspeck Mega Capturor 3D scanner.

In our experiment, we chose 3 face scans with neutral expressions to form the gallery set, making the gallery set have 315 samples. When forming the test set, two cases were considered. In the first case, the test set included all the remaining samples, while in the second case the test set only contained remaining frontal samples. Besides 3DMKDSRC, meshSIFT was also evaluated under the same experimental settings. The identification results in terms of rank-1 recognition rate are summarized in Table 1. In addition, results of several other algorithms are also reported. The methods described in [14, 15] both perform face recognition on regions that are more robust to expression variations (mainly the nose region). In [16], two baseline algorithms are implemented and validated, namely the Iterative Closest Point (ICP) algorithm and a method based on Principal Component Analysis (PCA) of depth images. It needs to be noted that experiments conducted in [14–16] were based on Bosphorus 2.0 which contains 2491 facial scans collected from 47 subjects, smaller than the one used in our experiments. In addition, only frontal samples were involved in those experiments.

From the results listed in Table 1, it can be seen that the proposed 3DMKDSRC performs much better than the other methods evaluated.

4.2. Experiments on GavabDB

GavabDB [22] is designed to be the most expression rich and noise prone 3D face database. It consists of laser range scans from 61 subjects. For each subject, 9 scans are collected, covering different poses and various facial expressions. We skipped those 2 types of scans which are largely rotated ($\pm$90 degrees). For each subject, we chose 3 neutral faces to build

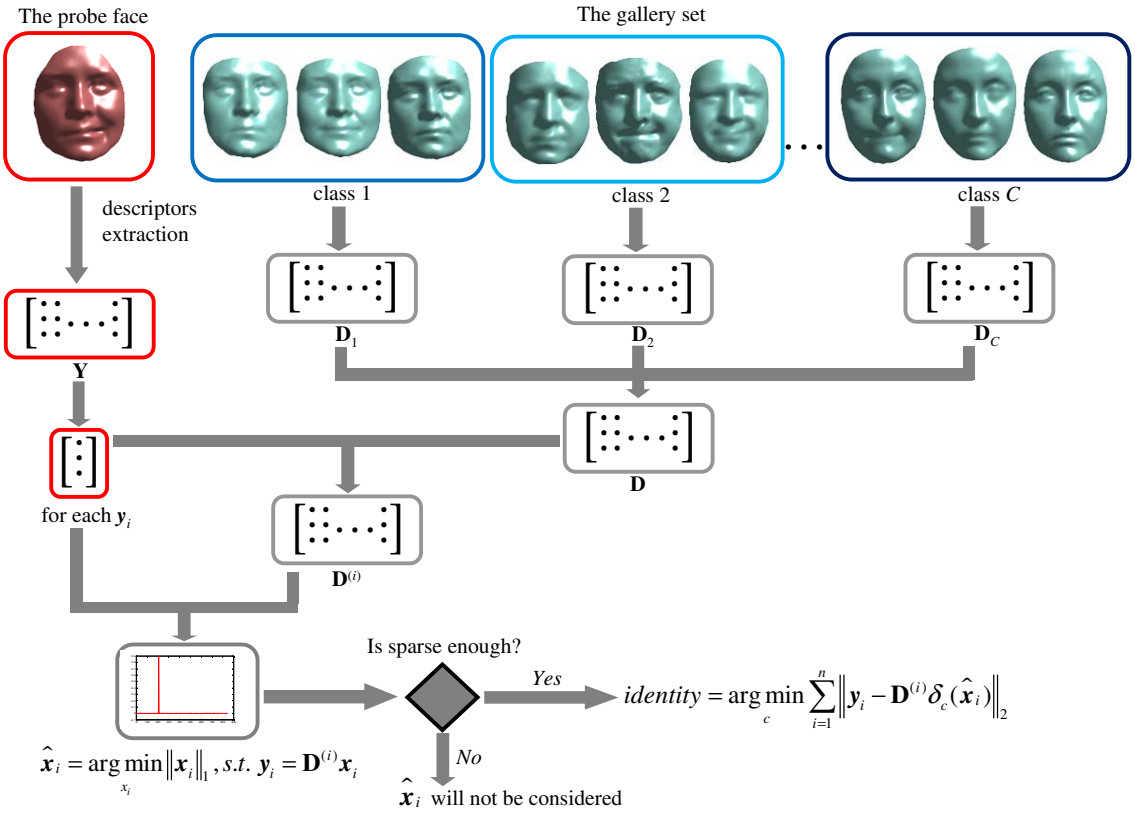

Fig. 6. The overall flowchart of 3DMKDSRC.

Table 1. Rank-1 recognition rates on Bosphorus.

Approach	Gallery size	Test size	Rank-1 RR
3DMKDSRC(all)	**315**	**4351**	**95.03%**
3DMKDSRC(frontal)	**315**	**3543**	**98.65%**
meshSIFT(all)	315	4351	92.99%
meshSIFT(frontal)	315	3543	96.56%
Hajati *et al*. [17](all)	-	-	69.1%
Dibeklioglu *et al*. [15](frontal)	47	1527	89.2%
Alyuz *et al*. [14](frontal)	47	1508	95.3%
ICP [16](frontal)	47	1508	72.4%
PCA [16](frontal)	47	1508	70.6%

Table 2. Rank-1 recognition rates on GavabDB.

Approach	Gallery size	Test size	Rank-1 RR
3DMKDSRC(neutral)	**183**	**61**	**100%**
3DMKDSRC(all)	**183**	**244**	**92.62%**
meshSIFT(neutral)	183	61	98.36%
meshSIFT(all)	183	244	86.22%
Moreno *et al*. [18](neutral)	60	60	78%
Moreno *et al*. [19](all)	305	122	77.9%
Mousavi *et al*. [20](neutral)	61	61	91%
Mahoor *et al*. [21](neutral)	61	183	95%

the gallery set. When forming the test set, two cases were considered. In the first case, the test set included all the remaining samples, while in the second case the test set only contained remaining neutral samples. Besides 3DMKDSRC, meshSIFT was also evaluated using the same experimental protocol. The rank-1 recognition rates are summarized in Table 2. In addition, results of several other representative algorithms are also reported in Table 2 for comparison.

The superiority of 3DMKDSRC over the other competitors can be clearly observed from the results in Table 2.

4.3. Experiments on FRGC2.0

FRGC2.0 [23] database contains 4007 3D range scans, taken from 466 different subjects.

In this experiment, we randomly chose 3 face scans for each subject to form the gallery set. For the subject which has less than 3 samples, we just put all its samples in the gallery. The rest of the faces in the database were used for testing. The rank-1 recognition rates obtained under those settings by 3DMKDSRC and meshSIFT are listed in Table 3. Actually, some state-of-the-art methods, such as [24], could achieve higher recognition accuracy than 3DMKDSRC on FRGC2.0. However, it should be noted that those methods would usually apply a complicated data preprocessing procedure (e.g.,

Table 3. Rank-1 recognition rates on FRGC2.0.

Approach	Gallery size	Test size	Rank-1 RR
3DMKDSRC	**1259**	**2748**	**89.29%**
meshSIFT	1259	2748	87.85%

hole filling) on the face scans in FRGC2.0 to improve the data quality. By contrast, in our experiments, no extra data preprocessing was performed. That's the main cause accounting for the lower recognition accuracies of 3DMKDSRC and meshSIFT reported here.

5. CONCLUSIONS

In this paper, we proposed a 3DMKDSRC approach for 3D face recognition. With 3DMKDSRC, each 3D face scan is represented by a set of descriptor vectors extracted from keypoints using meshSIFT. At the testing stage, a multitask SRC is used to determine the identity of a probe face scan. 3DMKDSRC is particular appropriate for matching range scans with missing parts, large expressions, or occlusions. Its efficacy has been corroborated by the extensive experiments conducted on various benchmark databases.

6. ACKNOWLEDGEMENT

This work is supported by NSFC under grant no. 61201394, the Shanghai Pujiang Program under grant no. 13PJ1408700, and the Innovation Program of Shanghai Municipal Education Commission under grant no. 12ZZ029.

References

[1] C. Dorai and A. Jain, "COSMOS-A representation scheme for 3D free-form objects," *IEEE Trans. PAMI*, vol. 19, no. 10, pp. 1115–1130, Oct. 1997.

[2] A. Mian, M. Bennamoun, and R. Owens, "An efficient multimodal 2D-3D hybrid approach to automatic face recognition," *IEEE Trans. PAMI*, vol. 29, no. 11, pp. 1927–1943, Nov. 2007.

[3] D. Smeets, J. Hermans, D. Vandermeulen, and P. Suetens, "Isometric deformation invariant 3D shape recognition," *Pattern Recognition*, vol. 45, no. 7, pp. 2817–2831, Jul. 2012.

[4] C.S. Chua and R. Jarvis, "Point signatures: A new representation for 3D object recognition," *Int. J. Comp. Vis.*, vol. 25, no. 1, pp. 63–85, Oct. 1997.

[5] M. Husken, M. Brauckmann, M. Gehlen, and C. Malsburg, "Strategies and benefits of fusion of 2D and 3D face recognition," in *CVPR Workshops*, 2005, pp. 174–174.

[6] Y. Wang, J. Liu, and X. Tang, "Robust 3D face recognition by local shape difference boosting," *IEEE Trans. PAMI*, vol. 32, no. 10, pp. 1858–1870, Oct. 2010.

[7] D.G. Lowe, "Distinctive image feature from scale-invariant keypoints," *Int. J. Comp. Vis.*, vol. 60, no. 2, pp. 91–110, Nov. 2004.

[8] D. Smeets, J. Keustermans, D. Vandermeulen, and P. Suetens, "MeshSIFT: Local surface features for 3D face recognition under expression variations and partial data," *CVIU*, vol. 117, no. 2, pp. 158–169, Feb. 2013.

[9] A. Savran, N. Alyuz, H. Dibekliglu, O. Celiktutan, B. Gokberk, B. Sankur, and L. Akarun, "Bosphorus database for 3D face analysis," in *Workshop on Biometrics and Identity Management*, 2008, pp. 47–56.

[10] J. Wright, A. Yang, A. Ganesh, S. Sastry, and Y. Ma, "Robust face recognition via sparse representation," *IEEE Trans. PAMI*, vol. 31, no. 2, pp. 210–227, Feb. 2009.

[11] S. Liao, A.K. Jain, and S.Z. Li, "Partial face recognition: An alignment-free approach," *IEEE Trans. PAMI*, vol. 35, no. 5, pp. 1193–1205, May 2013.

[12] D. Donoho, "For most large underdetermined systems of linear equations the minimal l_1-norm solution is also the sparsest solution," *Comm. Pure and Applied Math.*, vol. 59, no. 6, pp. 797–829, Jun. 2006.

[13] D. Donoho and Y. Tsaig, "Fast solution of l_1-norm minimization problem when the solution may be sparse," *IEEE Trans. Information Theory*, vol. 55, no. 11, pp. 4789–4812, Nov. 2008.

[14] N. Alyuz, B. Gokberk, and L. Akarun, "A 3D face recognition system for expressions and occlusion invariance," in *BTAS*, 2008, pp. 1–7.

[15] H. Dibekliglu, B. Gokberk, and L. Akarun, "Nasal region-based 3D face recognition under pose and expression variations," in *ICB*, 2009, pp. 309–318.

[16] N. Alyuz, B. Gokberk, H. Dibekliglu, A. Savran, A.A. Salah, L. Akarun, and B. Sankur, "3D face recognition benchmarks on the bosphorus database with focus on facial expressions," in *BIOID*, 2008, pp. 57–66.

[17] F. Hajati, A.A. Raie, and Y. Gao, "2.5D face recognition using patch geodesic moments," *Pattern Recognition*, vol. 45, no. 3, pp. 969–982, Mar. 2012.

[18] A.B. Moreno, A. Sanchez, J.F. Velez, and F.J. Diaz, "Face recognition using 3D surface-extracted descriptors," in *IMVIP*, 2003.

[19] A.B. Moreno, A. Sanchez, J.F. Velez, and F.J. Diaz, "Face recognition using 3D local geometrical features: PCA vs. SVM," in *Int. Sym. Image Signal Process. Anal.*, 2005, pp. 185–190.

[20] M.H. Mousavi, K. Faez, and A. Asghari, "Three dimensional face recognition using SVM classifier," in *ICIS*, 2008, pp. 208–213.

[21] M.H. Mahoor and M. Abdel-Mottaleb, "Face recognition based on 3D ridge images obtained from range data," *Pattern Recognition*, vol. 42, no. 3, pp. 445–451, Mar. 2009.

[22] A.B. Moreno and A. Sanchez, "Gavabdb: A 3D face database," 2004, http://gavab.escet.urjc.es.

[23] P.J. Phillips, P.J. Flynn, T. Scruggs, K.W. Bowyer, J. Chang, K. Hoffman, J. Marques, J. Min, and W. Worek, "Overview of the face recognition grand challenge," in *CVPR*, 2005, pp. 20–25.

[24] H. Drira, B.B. Amor, A. Srivastava, M. Daoudi, and R. Slama, "3D face recognition under expressions, occlusions, and pose variations," *IEEE Trans. PAMI*, vol. 35, no. 9, pp. 2270–2283, Sep. 2013.